Wave propagation in a FitzHugh-Nagumo-type model with modified excitability

E. P. Zemskov[1,2,*] and I. R. Epstein[1,†]

[1]*Department of Chemistry, Brandeis University, MS 015, Waltham, Massachusetts 02454, USA*
[2]*Computing Centre of the Russian Academy of Sciences, Vavilova 40, 119333 Moscow, Russia*

We examine a generalized FitzHugh-Nagumo (FHN) type model with modified excitability derived from the diffusive Morris-Lecar equations for neuronal activity. We obtain exact analytic solutions in the form of traveling waves using a piecewise linear approximation for the activator and inhibitor reaction terms. We study the existence and stability of waves and find that the inhibitor species exhibits different types of wave forms (fronts and pulses), while the activator wave maintains the usual kink (front) shape. The nonequilibrium Ising-Bloch bifurcation for the wave speed that occurs in the FHN model, where the control parameter is the ratio of inhibitor to activator time scales, persists when the strength of the inhibitor nonlinearity is taken as the bifurcation parameter.

I. INTRODUCTION

Wave propagation and pattern formation in a variety of excitable media can be effectively described by reaction-diffusion equations. One of the simplest two-component systems is the FitzHugh-Nagumo (FHN) [1] model,

$$\frac{\partial u}{\partial t} = u(1-u)(u-a) - v + D_u \frac{\partial^2 u}{\partial x^2}, \tag{1}$$

$$\frac{\partial v}{\partial t} = \varepsilon(u-v) + D_v \frac{\partial^2 v}{\partial x^2}, \tag{2}$$

where u and v are the activator and inhibitor variables, respectively; and the excitation threshold, a, the ratio of time scales, ε, and the diffusion coefficients, D_u and D_v, are constants. This model has been widely studied as a qualitative prototype for excitable systems in many biological [2] and chemical [3] contexts. Its piecewise linear caricature, the Rinzel-Keller [4] model,

$$\frac{\partial u}{\partial t} = -u - v + \theta(u-a) + D_u \frac{\partial^2 u}{\partial x^2}, \tag{3}$$

$$\frac{\partial v}{\partial t} = \varepsilon(u-v) + D_v \frac{\partial^2 v}{\partial x^2}, \tag{4}$$

allows for analytic solution by replacing the nonlinear term in Eq. (1) with the Heaviside function, $\theta(u-a)$.

To take into account the nonlinear dependence of the inhibitor reaction term that appears in more complicated models [5,6] (which are related to Morris-Lecar [7] type neuron models), Tonnelier and Gerstner [8] generalized the Rinzel-Keller equations and suggested a simple double piecewise linear variant

$$\frac{du}{dt} = -u/\tau - v + \mu\theta(u-a) + I, \tag{5}$$

$$\frac{dv}{dt} = b[\alpha\theta(u-a) - v]. \tag{6}$$

Here, the piecewise linear function in the first equation approximates the cubic nonlinearity in the activator kinetics, while the terms in the second equation mimic the sigmoidal function that describes [9] the behavior of the inhibitor variable in the Morris-Lecar model.

We consider here a general reaction-diffusion model, which includes both the Rinzel-Keller and the Tonnelier-Gerstner models as particular cases, i.e.,

$$\frac{\partial u}{\partial t} = -\alpha u - v + \theta(u-a) + \frac{\partial^2 u}{\partial x^2}, \tag{7}$$

$$\frac{\partial v}{\partial t} = \varepsilon[\bar{\alpha}u - v - \beta\theta(u-a)] + \frac{\partial^2 v}{\partial x^2}. \tag{8}$$

Equations (7) and (8) correspond to the Rinzel-Keller model with piecewise linear inhibition. The null clines for this model are shown in Fig. 1 for $\beta > 0$. This parameter characterizes the difference between the linear inhibition kinetics in classical FHN type systems, where $\beta = 0$, and the nonlinear Tonnelier-Gerstner form, which is obtained when $\bar{\alpha} = 0$ and $\beta < 0$. We can also obtain a system composed of two coupled Nagumo-type equations [10] when $\alpha = \bar{\alpha} = \beta = 1$.
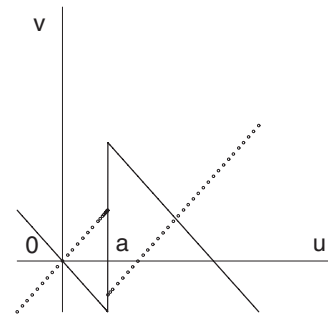

FIG. 1. Null clines for the model (7) and (8) with $\beta > 0$. Solid line: activator null-cline $-\alpha u - v + \theta(u-a) = 0$; dotted line: inhibitor null cline $\bar{\alpha}u - v - \beta\theta(u-a) = 0$.

─────────
*zemskov@brandeis.edu; zemskov@ccas.ru
†epstein@brandeis.edu

In an earlier study of a Rinzel-Keller-type model with equal diffusion coefficients [11], we developed techniques for obtaining exact solutions for propagating fronts, the front velocity and the growth rate of disturbances, i.e., the stability of fronts. Recently [12], we examined a simple piecewise linear reaction-diffusion model that possesses a front solution and used these methods to explore the effects of cross-diffusion, which may be relevant in both neuronal and ecological systems. Our goal here is to study the wave dynamics associated with a more general nonlinearity of the inhibitor reaction function than in the Tonnelier-Gerstner case. Thus, we extend the values of β into the positive range. We find a variety of propagation phenomena and explore in some detail the nonequilibrium Ising-Bloch bifurcation from stationary to propagating fronts.

In Sec. II, we outline our method for obtaining analytic solutions for fronts in models of this type and present explicit solutions for several cases. In Sec. III, we obtain an expression for the front speed and examine how that speed varies with the inhibitor nonlinearity β. In Sec. IV, we investigate the stability of the solutions obtained and apply these results to consideration of the Ising-Bloch bifurcation. Section V contains a brief summary and conclusion.

II. CONSTRUCTION OF TRAVELING WAVES

We look for traveling waves that approach constant concentrations at infinity. Introducing the traveling wave coordinate $\xi = x - ct$, where c is the wave speed, we can replace the original PDEs [Eqs. (7) and (8)] by a set of ODEs

$$\frac{d^2u}{d\xi^2} + c\frac{du}{d\xi} - \alpha u - v + \theta(u - a) = 0, \qquad (9)$$

$$\frac{d^2v}{d\xi^2} + c\frac{dv}{d\xi} + \varepsilon[\bar{\alpha}u - v - \beta\theta(u - a)] = 0. \qquad (10)$$

We seek a general solution as a sum of four exponentials, $u(\xi) = \Sigma A_n \exp(\lambda_n \xi) + u^*$, $v(\xi) = \Sigma B_n \exp(\lambda_n \xi) + v^*$, where $A_n, B_n (n = 1, \ldots, 4)$ are integration constants and u^*, v^* are constants to which the solution tends at infinity. The four eigenvalues λ_n may be found by the method introduced in Ref. [11]. We obtain

$$\lambda_{1,2} = -c/2 + \rho_{1,2}, \quad \lambda_{3,4} = -c/2 - \rho_{1,2} \qquad (11)$$

with

$$\rho_{1,2} = \sqrt{c^2/4 + (\varepsilon + \alpha)/2 \pm \sqrt{(\varepsilon + \alpha)^2/4 - \varepsilon(\alpha + \bar{\alpha})}}. \qquad (12)$$

The constants B_n can be expressed in terms of the A_n as $B_n = (\lambda_n^2 + c\lambda_n - \alpha)A_n$, or

$$B_{1,3} = \mu_1 A_{1,3}, \quad B_{2,4} = \mu_2 A_{2,4}, \qquad (13)$$

where

$$\mu_{1,2} = (\varepsilon - \alpha)/2 \pm \sqrt{(\varepsilon - \alpha)^2/4 - \varepsilon\bar{\alpha}}. \qquad (14)$$

To construct the front solutions from the two pieces valid on either side of the jump point, a, we must take into account the signs of the λ_n. Since ε and α are positive, $\lambda_{1,2} > 0$ and

$\lambda_{3,4} < 0$, so the front solutions, which must approach the steady state values, $(0,0)$ and (u^*, v^*) at $-\infty$ and $+\infty$, respectively, are

$$u_1(\xi) = A_1 e^{\lambda_1 \xi} + A_2 e^{\lambda_2 \xi},$$

$$v_1(\xi) = B_1 e^{\lambda_1 \xi} + B_2 e^{\lambda_2 \xi}, \quad \xi \le \xi_a, \qquad (15)$$

$$u_2(\xi) = A_3 e^{\lambda_3 \xi} + A_4 e^{\lambda_4 \xi} + u^*,$$

$$v_2(\xi) = B_3 e^{\lambda_3 \xi} + B_4 e^{\lambda_4 \xi} + v^*, \quad \xi \ge \xi_a. \qquad (16)$$

Here $u^* = (1 + \beta)/(\alpha + \bar{\alpha})$ and $v^* = (\bar{\alpha} - \alpha\beta)/(\alpha + \bar{\alpha})$.

For some values of ε and α, the simple exponential front solutions (15) and (16) take on a damped oscillatory character, because, as found in Ref. [11], there exists a range of ε and α where the eigenvalues λ_n become complex. For $\bar{\alpha} = 1$, when $\varepsilon_{\text{im}}^- < \varepsilon < \varepsilon_{\text{im}}^+$, where $\varepsilon_{\text{im}}^\pm = \alpha + 2 \pm 2\sqrt{\alpha + 1}$, the λ_n have nonzero imaginary parts, so that the functions $u(\xi)$ and $v(\xi)$ contain cosine and sine terms.

In the Rinzel-Keller case we have $\alpha = \bar{\alpha} = 1$ and $\beta = 0$. Then

$$\rho_{1,2} = \sqrt{c^2/4 + (\varepsilon + 1)/2 \pm \sqrt{(\varepsilon + 1)^2/4 - 2\varepsilon}}, \qquad (17)$$

$$\mu_{1,2} = (\varepsilon - 1)/2 \pm \sqrt{(\varepsilon - 1)^2/4 - \varepsilon} \qquad (18)$$

and $u^* = v^* = 1/2$. This case was studied in detail in Ref. [11].

In the Tonnelier-Gerstner case we set $\bar{\alpha} = 0$ and $\beta < 0$. In this situation $\mu_1 = 0$ and $\mu_2 = \varepsilon - \alpha < 0$ since we usually choose $\alpha = 1$ and the ratio of the time scales is already very small, $\varepsilon \ll 1$. Hence

$$\rho_1 = \sqrt{c^2/4 + \alpha}, \quad \rho_2 = \sqrt{c^2/4 + \varepsilon} \approx c/2 \qquad (19)$$

and $u^* = (1 + \beta)/\alpha$, $v^* = -\beta$. Thus, the traveling fronts in this case always have nonoscillatory tails. The front profiles in the Tonnelier-Gerstner case have shapes similar to the FHN model and we do not discuss them in detail here.

III. SPEED EQUATIONS

The analytic solutions discussed above are constructed on two half-lines and must be matched where they meet. Requiring the continuity of the functions $u(\xi), v(\xi)$ and their derivatives yields five equations, with the fifth equation fixing the matching point, $u(0) = a$, where $\xi_a = 0$ is chosen,

$$A_1 + A_2 = a, \quad A_3 + A_4 + u^* = a,$$

$$A_1\lambda_1 + A_2\lambda_2 = A_3\lambda_3 + A_4\lambda_4,$$

$$A_1\mu_1 + A_2\mu_2 = A_3\mu_1 + A_4\mu_2 + v^*,$$

$$A_1\mu_1\lambda_1 + A_2\mu_2\lambda_2 = A_3\mu_1\lambda_3 + A_4\mu_2\lambda_4. \qquad (20)$$

Eliminating the constants A_n, we reduce the number of equations from five to one and after introducing Eq. (11), simple algebra yields the following equation for the speed c:
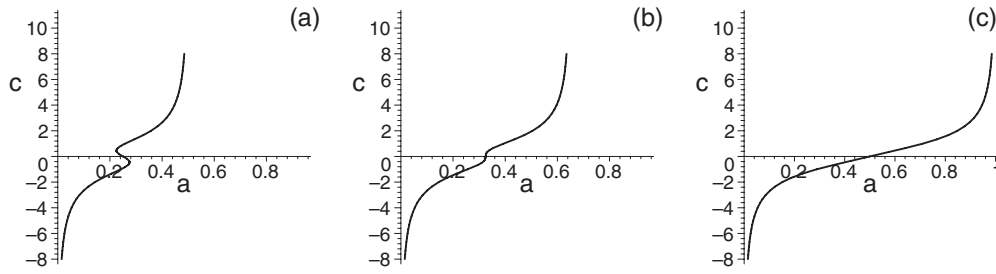
FIG. 2. Speed diagrams. Wave speed vs excitation threshold at (a) $\beta=0$ (the Rinzel-Keller model), (b) $\beta=0.3$ and (c) $\beta=1$ (two coupled Nagumo equations). Parameters: $\alpha=\bar{\alpha}=1$ and $\varepsilon=0.1$.

$$\frac{c}{2}u^*(\rho_1\mu_1-\rho_2\mu_2)-\frac{c}{2}v^*(\rho_1-\rho_2)+\rho_1\rho_2(\mu_1-\mu_2)(u^*-2a)$$
$$=0. \qquad (21)$$

Here we have taken into account that $\mu_1\neq\mu_2$. From this speed equation it follows directly that there exists a motionless front ($c=0$) when the system is symmetric ($a=u^*/2$). From Eq. (21) one can express the threshold a as

$$a=\frac{u^*}{2}+\frac{c}{4}\frac{1}{\rho_1\rho_2(\mu_1-\mu_2)}[u^*(\rho_1\mu_1-\rho_2\mu_2)-v^*(\rho_1-\rho_2)]. \qquad (22)$$

In the Rinzel-Keller model, because $u^*=v^*=1/2$, the speed Eq. (22) reduces to

$$a=\frac{1}{4}+\frac{c}{8}\frac{1}{\rho_1\rho_2(\mu_1-\mu_2)}[(\rho_1\mu_1-\rho_2\mu_2)-(\rho_1-\rho_2)] \qquad (23)$$

and the symmetry condition is $a=1/4$. The front speed behavior for the FHN model and its piecewise linear approximation are well known [4,13,14] and are not discussed further here.

In the Tonnelier-Gerstner case, using the fact that $\mu_1=0$, we can write the speed Eq. (22) in the form

$$a=\frac{u^*}{2}\left(1+\frac{c}{2}\frac{1}{\rho_1}\right)+\frac{c}{4}\frac{v^*}{\mu_2}\left(\frac{1}{\rho_2}-\frac{1}{\rho_1}\right). \qquad (24)$$

There is an additional special case (two coupled Nagumo equations) with symmetric null clines, i.e., when $\alpha=\bar{\alpha}=\beta=1$ in Eqs. (7) and (8). Here $u^*=1$ and $v^*=0$ and the speed equation becomes

$$a=\frac{1}{2}+\frac{c}{4}\frac{\rho_1\mu_1-\rho_2\mu_2}{\rho_1\rho_2(\mu_1-\mu_2)}. \qquad (25)$$

The symmetric situation appears here when $a=1/2$.

The speed diagrams, c vs a, described by Eq. (22) for $\alpha=\bar{\alpha}=1$ and $\varepsilon=0.1$ and at fixed values of β, are shown in Fig. 2. In Fig. 2(a) the $c-a$ curve folds to form three connected branches, i.e., a bifurcation occurs as we vary the control parameter a. This bifurcation has been referred to in the literature as a nonequilibrium Ising-Bloch bifurcation [14,15]. As the influence of the nonlinearity of the inhibition, β, grows, the folded region of the curve narrows and unfolds [see Fig. 2(b)] when $\beta=1$ [Fig. 2(c)]. The same bifurcation

scenario is found when the bifurcation parameter is chosen as the ratio of time scales, ε. On the $c-\varepsilon$ diagram the bifurcation appears as a pitchfork curve. In the additional special case [Eq. (25)] the front speed behavior is very simple and corresponds to that shown in Fig. 2(c). The speed diagrams for the Tonnelier-Gerstner case, c vs a, show the same bifurcation scenario as in the above-described general case. The nonequilibrium Ising-Bloch bifurcation now occurs when the parameter β becomes negative.

The corresponding wave profiles are shown in Figs. 3–6. In Fig. 3 the activator front $u=u(\xi)$ with nonoscillatory tails is presented; the corresponding inhibitor front $v=v(\xi)$ is illustrated by Fig. 5(a). In Fig. 4 the activator front has oscillatory tails; the related inhibitor front is shown in Fig. 6(a). Figures 5(b), 5(c), 6(b), and 6(c) represent the inhibitor waves for different parameter values. The corresponding activator profiles are similar to those shown in Figs. 3 and 4 and are not displayed here.

In Figs. 3 and 5 the ratio of the time scales is $\varepsilon=0.1$, and the slope of the activator null cline is $\alpha=1$, so that the fronts have nonoscillatory tails. When β is small the fronts are similar in shape to the classical FHN fronts. But when β is large enough (>0.5) the profile of the inhibitor front becomes nonmonotonic [Fig. 5(a)], whereas the activator profile remains the same. Moreover, for $\beta=1$ we obtain a front-pulse combination of waves: the activator wave is still associated with a front (heteroclinic-type wave), but the inhibitor wave is represented now by a homoclinic-type curve or pulse [Figs. 5(b) and 5(c)]. Similar combinations of this front-pulse type were described recently by Berezovskaya *et al.* [16] in models with cross-diffusion. In Figs. 5(a) and 5(c)
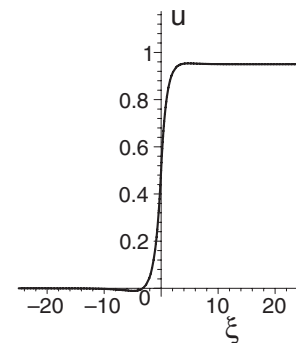

FIG. 3. Traveling wave solution with nonoscillatory tails for the activator variable $u=u(\xi)$. $a=0.5$, $\alpha=1$, $\bar{\alpha}=1$, $\beta=0.9$, and $\varepsilon=0.1$. The calculated speed is $c\approx0.134$.
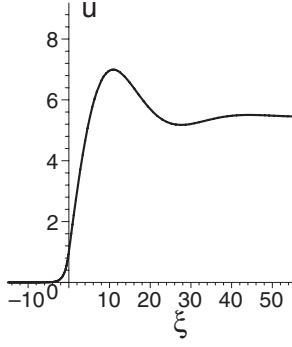
FIG. 4. Traveling wave solution with oscillatory tails for the activator variable $u=u(\xi)$. $a=1$, $\alpha=0.1$, $\bar{\alpha}=1$, $\beta=5$, and $\varepsilon=0.05$. The calculated speed is $c\approx-0.975$.

the fronts propagate with positive speed, i.e., from left to right. When $u^*=2a$ the speed value is equal to zero, the fronts are motionless [Fig. 5(b)].

In Figs. 4 and 6 the values of the basic parameters are chosen to yield waves with oscillatory tails. The ratio of time scales is fixed at $\varepsilon=0.05$, and the slope of the activator null cline is $\alpha=0.1$. The characteristic features of the fronts with oscillatory tails remain the same as in the FHN case: (i) the oscillations are behind the front and (ii) the trajectory in the $u-v$ plane is a spiral, as described in Ref. [17].

IV. STABILITY ANALYSIS

To investigate the stability of the solutions $u(\xi)$ and $v(\xi)$, we consider a perturbation of the form $\Delta u(\xi,y,t)$ $=\tilde{u}(\xi)\exp(\omega t+iky)$ and $\Delta v(\xi,y,t)=\tilde{v}(\xi)\exp(\omega t+iky)$, where y is the direction transverse to the direction of propagation of the planar front, and ω and k are the growth rate and the wave number, respectively. A linear stability analysis assumes perturbed solutions of the form

$$U(\xi,y,t) = u(\xi) + \Delta u(\xi,y,t),$$

$$V(\xi,y,t) = v(\xi) + \Delta v(\xi,y,t), \quad (26)$$

where the small perturbations $\Delta u(\xi,y,t)$ and $\Delta v(\xi,y,t)$ are added to the planar front solutions. In the stationary frame, the full perturbed solutions satisfy

$$\frac{\partial U}{\partial t} = \frac{\partial^2 U}{\partial \xi^2} + \frac{\partial^2 U}{\partial y^2} + f(U,V),$$

$$\frac{\partial V}{\partial t} = \frac{\partial^2 V}{\partial \xi^2} + \frac{\partial^2 V}{\partial y^2} + g(U,V) \quad (27)$$

and $u(\xi)$, $v(\xi)$ are time-independent solutions of these equations. Subtracting the equations for the unperturbed solutions and linearizing for small Δu and Δv, we obtain the variational equations for the perturbations

$$\frac{\partial \Delta u}{\partial t} = \frac{\partial^2 \Delta u}{\partial \xi^2} + \frac{\partial^2 \Delta u}{\partial y^2} + \frac{\partial f}{\partial u}\Delta u + \frac{\partial f}{\partial v}\Delta v,$$

$$\frac{\partial \Delta v}{\partial t} = \frac{\partial^2 \Delta v}{\partial \xi^2} + \frac{\partial^2 \Delta v}{\partial y^2} + \frac{\partial g}{\partial u}\Delta u + \frac{\partial g}{\partial v}\Delta v. \quad (28)$$

The equations for the eigenfunctions (the variational equations) read

$$\frac{d^2\tilde{u}}{d\xi^2} + c\frac{d\tilde{u}}{d\xi} - [\tilde{\alpha} - \delta(u-a)]\tilde{u} - \tilde{v} = 0,$$

$$\frac{d^2\tilde{v}}{d\xi^2} + c\frac{d\tilde{v}}{d\xi} + \varepsilon[\bar{\alpha} - \beta\delta(u-a)]\tilde{u} - \varepsilon\tilde{\varepsilon}\tilde{v} = 0, \quad (29)$$

where $\tilde{\alpha}=\alpha+\omega+k^2$ and $\tilde{\varepsilon}=\varepsilon+\omega+k^2$.

Inserting the perturbation solutions in the form $\tilde{u}$, $\tilde{v}(\xi)$ $=\Sigma\tilde{A}$, $\tilde{B}\exp(\tilde{\lambda}\xi)$ into the variational Eqs. (29) we obtain the following matrix equation:

$$\begin{pmatrix} \tilde{\gamma}-\tilde{\alpha} & -1 \\ \varepsilon\bar{\alpha} & \tilde{\gamma}-\tilde{\varepsilon} \end{pmatrix}\begin{pmatrix} \tilde{A} \\ \tilde{B} \end{pmatrix} = 0 \quad (30)$$

with $\tilde{\gamma}=\tilde{\lambda}^2+c\tilde{\lambda}$. Hence the characteristic equation is $\tilde{\gamma}^2-(\tilde{\varepsilon}+\tilde{\alpha})\tilde{\gamma}+\tilde{\varepsilon}\tilde{\alpha}+\varepsilon\bar{\alpha}=0$, with roots

$$\tilde{\gamma}_{1,2} = (\tilde{\varepsilon}+\tilde{\alpha})/2 \pm \sqrt{(\varepsilon-\alpha)^2/4-\varepsilon\bar{\alpha}} \quad (31)$$

so that $\tilde{\gamma}_{1,2}-\tilde{\alpha}=\mu_{1,2}$ and

$$\tilde{B}_{1,3} = \mu_1\tilde{A}_{1,3}, \quad \tilde{B}_{2,4} = \mu_2\tilde{A}_{2,4}, \quad (32)$$

The perturbations $\tilde{u}(\xi)$ and $\tilde{v}(\xi)$ should be matched as was done for the wave solutions. However, now the matching conditions for the derivatives have jumps due to the delta function in the variational equations. To make use of this behavior, we integrate the variational equations over a small
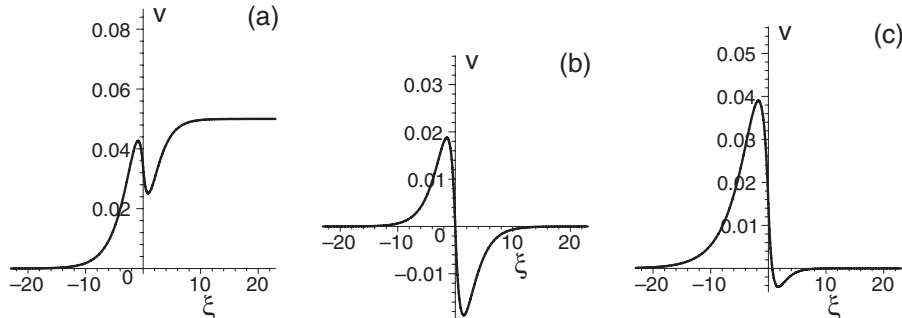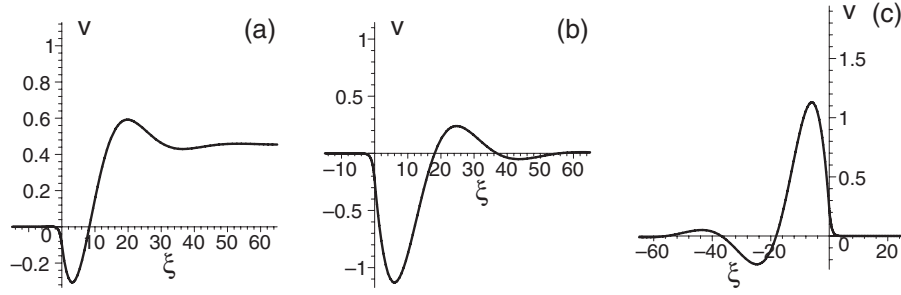

FIG. 5. Traveling wave solutions with nonoscillatory tails for the inhibitor (recovery variable) $v=v(\xi)$. $\alpha=1$, $\bar{\alpha}=1$, $\varepsilon=0.1$ and (a) $a=0.5$, $\beta=0.9$, (b) $a=0.5$, $\beta=1$, (c) $a=0.6$, $\beta=1$. The speed is: (a) $c\approx0.134$, (b) $c=0$ and (c) $c\approx0.459$.

FIG. 6. Traveling wave solutions with oscillatory tails for the inhibitor (recovery variable) $v = v(\xi)$. $\alpha = 0.1$, $\bar{\alpha} = 1$, $\varepsilon = 0.05$ and (a) $a = 1$, $\beta = 5$, (b) $a = 1$, $\beta = 10$, (c) $a = 9$, $\beta = 10$. The speed is: (a) $c \approx -0.975$, (b) $c \approx -1.163$ and (c) $c \approx 1.163$.

interval about the matching point of the perturbations. Nonzero contributions arise from the diffusive terms and terms containing the delta function, i.e.,

$$\frac{d\tilde{u}}{d\xi}\bigg|_{0-}^{0+} + \int_{0-}^{0+} \frac{\delta(\xi)}{|du(0)/d\xi|}\tilde{u}\,d\xi = 0 \tag{33}$$

for the first equation in Eq. (29) and

$$\frac{d\tilde{v}}{d\xi}\bigg|_{0-}^{0+} - \varepsilon\beta \int_{0-}^{0+} \frac{\delta(\xi)}{|du(0)/d\xi|}\tilde{u}\,d\xi = 0 \tag{34}$$

for the second one. After the integration of the delta function we can rewrite the last two equations as

$$d\tilde{u}_1(0)/d\xi = d\tilde{u}_2(0)/d\xi + \tilde{u}_0/|du(0)/d\xi|,$$

$$d\tilde{v}_1(0)/d\xi = d\tilde{v}_2(0)/d\xi - \varepsilon\beta\tilde{u}_0/|du(0)/d\xi|, \tag{35}$$

where $\tilde{u}_0 = \text{const}$ is a perturbation amplitude. The other matching equations are $\tilde{u}_1(0) = \tilde{u}_2(0)$, $\tilde{v}_1(0) = \tilde{v}_2(0)$, and $\tilde{u}_1(0) = \tilde{u}_0$.

Eliminating $\tilde{A}$ from the matching conditions, we obtain the growth rate equation

$$(\mu_1\tilde{\rho}_1 - \mu_2\tilde{\rho}_2) + \varepsilon\beta(\tilde{\rho}_1 - \tilde{\rho}_2) - 2\tilde{\rho}_1\tilde{\rho}_2(\mu_1 - \mu_2)|du(0)/d\xi| = 0, \tag{36}$$

with

$$\tilde{\rho}_{1,2} = \sqrt{\frac{c^2}{4} + \omega + k^2 + \frac{\varepsilon + \alpha}{2} \pm \sqrt{\frac{(\varepsilon + \alpha)^2}{4} - \varepsilon(\alpha + \bar{\alpha})}}. \tag{37}$$

Thus, the growth rate equation has the form $F(\omega + k^2, \varepsilon, \alpha, \bar{\alpha}, \beta) = 0$. From this fact it follows that the fastest growing mode will always correspond to $k = 0$, and we may then restrict ourselves to the $k = 0$ case as we did in Ref. [11]. Moreover, the combination $\omega + k^2$ appears in all expressions for the eigenvalues $\tilde{\lambda}$ and the perturbations $\tilde{u}(\xi)$ and $\tilde{v}(\xi)$.

The stability analysis generalizes the results which were obtained for the Rinzel-Keller model. The stability criteria are similar, because the underlying front speed bifurcation, the Ising-Bloch bifurcation, remains the same. At this bifurcation, a pair of counterpropagating fronts arises instead of a single stationary front. The stationary front becomes unstable, whereas the two moving fronts are stable. This instability corresponds to the real eigenvalue (the growth rate ω) crossing zero. Because the nonequilibrium Ising-Bloch bifurcation remains the same as in the Rinzel-Keller case, we omit a more detailed discussion here.

V. SUMMARY AND CONCLUSION

Wave propagation from the perspective of reaction-diffusion systems has been studied based on exact analytic solutions for the traveling waves obtained using piecewise linear approximations for the reaction terms. The main result of the paper is a description of the diverse wave forms in FHN-type systems with modified excitability (nonlinear inhibition). We find that a nonequilibrium bifurcation of the Ising-Bloch type for the wave speed disappears when the nonlinearity in the inhibitor reaction function grows. This type of bifurcation determines the excitable properties of the system and hence the wave propagation in the medium. Such wave propagation may lead to complex pattern formation in a variety of 2D systems [14].

The reaction-diffusion model considered here differs from the classical Morris-Lecar model developed to describe oscillations in the giant muscle fiber of barnacles. Because it has biophysically meaningful and measurable parameters, that model has become quite popular in the computational neuroscience community. The mixed form discussed in our paper is mathematically easier to treat and can be extended to generalize the FHN equations by taking into account the nonlinear inhibition kinetics (as in Refs. [5,18]) similar to the behavior of the recovery variable in the Morris-Lecar case. The model presented here can exhibit various types of traveling waves and may be considered as a starting point for more elaborate investigations.

[1] R. FitzHugh, Biophys. J. **1**, 445 (1961); J. Nagumo, S. Arimoto, and S. Yoshizawa, Proc. IRE **50**, 2061 (1962).

[2] J. D. Murray, *Mathematical Biology*, 3rd ed. (Springer, Berlin, 2003).

[3] A. S. Mikhailov and K. Showalter, Phys. Rep. **425**, 79 (2006).

[4] J. Rinzel and J. B. Keller, Biophys. J. **13**, 1313 (1973); J. Rinzel and D. Terman, SIAM J. Appl. Math. **42**, 1111 (1982).

[5] V. B. Kazantsev, Phys. Rev. E **64**, 056210 (2001).

[6] S. Coombes, SIAM J. Appl. Dyn. Syst. **7**, 1101 (2008).

[7] C. Morris and H. Lecar, Biophys. J. **35**, 193 (1981).

[8] A. Tonnelier and W. Gerstner, Phys. Rev. E **67**, 021908 (2003).

[9] H. G. Rotstein, N. Kopell, A. M. Zhabotinsky, and I. R. Epstein, SIAM J. Appl. Math. **63**, 1998 (2003); J. Chem. Phys. **119**, 8824 (2003).

[10] V. I. Nekorkin, V. B. Kazantsev, S. Morfu, J. M. Bilbault, and P. Marquié, Phys. Rev. E **64**, 036602 (2001).

[11] E. P. Zemskov, V. S. Zykov, K. Kassner, and S. C. Müller, Nonlinearity **13**, 2063 (2000).

[12] E. P. Zemskov and A. Yu. Loskutov, J. Exp. Theor. Phys. **107**, 344 (2008).

[13] A. Ito and T. Ohta, Phys. Rev. A **45**, 8374 (1992).

[14] A. Hagberg and E. Meron, Phys. Rev. E **48**, 705 (1993); Phys. Rev. Lett. **72**, 2494 (1994); Nonlinearity **7**, 805 (1994).

[15] P. Coullet, J. Lega, B. Houchmanzadeh, and J. Lajzerowicz, Phys. Rev. Lett. **65**, 1352 (1990).

[16] F. S. Berezovskaya, A. S. Novozhilov, and G. P. Karev, Nonlinear Anal.: Real World Appl. **9**, 1866 (2008).

[17] E. P. Zemskov, V. S. Zykov, K. Kassner, and S. C. Müller, Physica D **183**, 117 (2003).

[18] V. I. Nekorkin, A. S. Dmitrichev, J. M. Bilbault, and S. Binczak, Physica D **239**, 972 (2010).